J|A|C|S ARTICLES

Published on Web 09/29/2010

Understanding the Stabilization of Liquid-Phase-Exfoliated Graphene in Polar Solvents: Molecular Dynamics Simulations and Kinetic Theory of Colloid Aggregation

Chih-Jen Shih,[†] Shangchao Lin,[†,‡] Michael S. Strano,[†] and Daniel Blankschtein*[,†]

Departments of Chemical and Mechanical Engineering, Massachusetts Institute of Technology, Cambridge, Massachusetts 02139, United States

Received July 20, 2010; E-mail: dblank@mit.edu

Abstract: Understanding the solution-phase dispersion of pristine, unfunctionalized graphene is important for the production of conducting inks and top-down approaches to electronics. This process can also be used as a higher-quality alternative to chemical vapor deposition. We have developed a theoretical framework that utilizes molecular dynamics simulations and the kinetic theory of colloid aggregation to elucidate the mechanism of stabilization of liquid-phase-exfoliated graphene sheets in *N*-methylpyrrolidone (NMP), *N*,*N*′-dimethylformamide (DMF), dimethyl sulfoxide (DMSO), γ-butyrolactone (GBL), and water. By calculating the potential of mean force between two solvated graphene sheets using molecular dynamics (MD) simulations, we have found that the dominant barrier hindering the aggregation of graphene is the last layer of confined solvent molecules between the graphene sheets, which results from the strong affinity of the solvent molecules for graphene. The origin of the energy barrier responsible for repelling the sheets is the steric repulsions between solvent molecules and graphene before the desorption of the confined single layer of solvent. We have formulated a kinetic theory of colloid aggregation to model the aggregation of graphene sheets in the liquid phase in order to predict the stability using the potential of mean force. With only one adjustable parameter, the average collision area, which can be estimated from experimental data, our theory can describe the experimentally observed degradation of the single-layer graphene fraction in NMP. We have used these results to rank the potential solvents according to their ability to disperse pristine, unfunctionalized graphene as follows: NMP $\approx$ DMSO > DMF > GBL > H_2O. This is consistent with the widespread use of the first three solvents for this purpose.

1. Introduction

The discovery of two-dimensional, one-atom-thick graphene in 2004[1] has generated considerable research effort aimed at demonstrating the outstanding electronic and mechanical properties of this unique material.[2−6] Fundamental investigations were carried out using micromechanically cleaved single-layer and bilayer graphene[7] from highly ordered pyrolytic graphite (HOPG), which unfortunately is not well-suited for industrial applications.[8] The demand for the development of large-scale, high-throughput methods for mass production of graphene has stimulated extensive investigation in recent years.[9] Although large-area graphene films have been produced by chemical vapor deposition (CVD) growth on metal substrates,[10] exfoliation of graphene in a liquid phase has shown its superiority for both scaling-up and allowing chemical functionalization of graphene.[8] In our opinion, liquid-phase exfoliation of graphene is potentially important for the production of conducting inks and top-down approaches to electronics. It can also be used as a higher-quality alternative to CVD. To date, reduced graphite oxides (RGOs),[11−13] graphite,[14−19] and graphite-intercalated compounds (GICs)[20−22] have been proposed as raw materials for liquid-phase production of graphene. In these production methods, the key challenge involves exfoliating these materials in a liquid that can disperse the graphene sheets in a stable manner.

A number of studies have reported the preparation of graphene dispersions in highly polar solvents,[9] such as *N*-methylpyrrolidone (NMP)[15] and *N*,*N*′-dimethylformamide (DMF).[14] The selection of these solvents was based primarily

[†] Department of Chemical Engineering.
[‡] Department of Mechanical Engineering.

(1) Novoselov, K. S.; Geim, A. K.; Morozov, S. V.; Jiang, D.; Zhang, Y.; Dubonos, S. V.; Grigorieva, I. V.; Firsov, A. A. *Science* **2004**, *306*, 666–669.
(2) Geim, A. K.; Novoselov, K. S. *Nat. Mater.* **2007**, *6*, 183–191.
(3) Affoune, A. M.; Prasad, B. L. V.; Sato, H.; Enoki, T.; Kaburagi, Y.; Hishiyama, Y. *Chem. Phys. Lett.* **2001**, *348*, 17–20.
(4) Manna, A. K.; Pati, S. K. *Chem.—Asian J.* **2009**, *4*, 855–860.
(5) Ghosh, A.; Subrahmanyam, K. S.; Krishna, K. S.; Datta, S.; Govindaraj, A.; Pati, S. K.; Rao, C. N. R. *J. Phys. Chem. C* **2008**, *112*, 15704–15707.
(6) Dutta, S.; Pati, S. K. *J. Mater. Chem.* **2010**, *20*, 8207–8223.
(7) Novoselov, K. S.; Jiang, D.; Schedin, F.; Booth, T. J.; Khotkevich, V. V.; Morozov, S. V.; Geim, A. K. *Proc. Natl. Acad. Sci. U.S.A.* **2005**, *102*, 10451–10453.
(8) Coleman, J. N. *Adv. Funct. Mater.* **2009**, *19*, 3680–3695.
(9) Park, S.; Ruoff, R. S. *Nat. Nanotechnol.* **2009**, *4*, 217–224.
(10) Sutter, P. W.; Flege, J. I.; Sutter, E. A. *Nat. Mater.* **2008**, *7*, 406–411.
(11) Niyogi, S.; Bekyarova, E.; Itkis, M. E.; McWilliams, J. L.; Hamon, M. A.; Haddon, R. C. *J. Am. Chem. Soc.* **2006**, *128*, 7720–7721.
(12) Stankovich, S.; Dikin, D. A.; Piner, R. D.; Kohlhaas, K. A.; Kleinhammes, A.; Jia, Y.; Wu, Y.; Nguyen, S. T.; Ruoff, R. S. *Carbon* **2007**, *45*, 1558–1565.
(13) Li, D.; Muller, M. B.; Gilje, S.; Kaner, R. B.; Wallace, G. G. *Nat. Nanotechnol.* **2008**, *3*, 101–105.

10.1021/ja1064284

on trial-and-error experimentation involving dispersions of carbon nanotubes.[23] Recently, Hernandez and co-workers[15,24] have shown that solvents that are efficient at dispersing graphene can be selected on the basis their Hildebrand solubility parameters, Hansen solubility parameters, and surface tensions. According to Hernandez and co-workers,[15,24] efficient solvents should have surface tensions equal to that of graphene in order to minimize the enthalpic cost of mixing.[15] Although this type of semiempirical criterion does provide useful preliminary information for testing existing solvents,[17] it does not permit molecular-level design[25] of new solvents that are capable of efficiently dispersing graphene. Moreover, in addition to optimal graphene solubility, the other key requirement for a solvent to efficiently disperse graphene is its ability to colloidally stabilize graphene. For this purpose, the graphene−solvent interactions should be sufficiently strong to compensate for the enormous van der Waals (vdW) attractive interactions that operate between the graphene sheets. In this respect, very little is known about the molecular details of the interactions between graphene and solvent molecules, including the correlation of these interactions with the solvent-induced colloidal stability of the graphene solution.[24] Accordingly, developing a molecular-level understanding of graphene−solvent interactions represents a very important step toward optimizing the design of stable solvent-induced graphene dispersions.

Because of the nonideal behavior exhibited by polar solvents, molecular dynamics (MD) simulations provide a promising computational tool for elucidating the nature of graphene−solvent interactions at the molecular level. The most common polar solvent, water, has been studied systematically. Specifically, Hummer et al.[26] showed that because of density fluctuations in the surrounding bulk-water phase, several water molecules tend to be confined inside a narrow hydrophobic carbon nanotube, although this leads to an increase in potential energy. In addition, Choudhury and Pettitt[27] proposed that for a specific range of intergraphene distances, a single layer of confined water molecules can form between two hydrophobic graphene sheets. This follows because the gain in the graphene−water vdW interaction energy may overcompensate for the loss of hydrogen bonds between the highly confined water molecules. Thus, optimal solvents that are capable of efficiently dispersing graphene in a more stable manner prefer to be more confined between the graphene sheets instead of remaining in the bulk-solvent phase. This should be a very important requirement used to select efficient solvents for production of stable graphene dispersions.

In the present work, with all of the above in mind, we studied for the first time the interactions of graphene with five polar solvents [water, DMF, NMP, dimethyl sulfoxide (DMSO), and γ-butyrolactone (GBL)] using large-scale MD simulations. The potential of mean force (PMF) between two parallel graphene sheets in each of these solvents was simulated in order to investigate the thermodynamic stability of the graphene dispersion in that solvent. The molecular-level origin of the confinement and desorption of the solvent molecules from the intersheet space was also investigated. In addition, to understand the kinetics of aggregation of graphene sheets in the various solvents, a novel theoretical approach combining the PMF results obtained using MD simulations with a kinetic theory of colloid aggregation was developed. With only one adjustable parameter, the average collision area, which can be estimated from experimental data, this combined theoretical framework can be utilized to predict the lifetime and time-dependent layer distribution of graphene in solvents. Moreover, we also utilized our theoretical methodology to rank the five solvents in terms of their graphene stabilizing ability, which, as stressed above, is extremely important in the selection of suitable efficient solvents. Finally, the investigation presented here also provides fundamental insight into the molecular-level design of efficient solvents to enhance the dispersion of graphene in the liquid phase.

2. Simulation Method

In the work presented here, we carried out MD simulations with the *NPT* ensemble (constant number of atoms N, constant pressure $P = 1.0$ bar, and constant temperature $T = 298.15$ K) using the GROMACS 4.0[28] software package and the *o*ptimized *p*otentials for *l*iquid *s*imulations−*a*ll *a*toms (OPLS-AA)[29] force field. All of the carbon atoms in graphene were treated as uncharged Lennard-Jones (LJ) spheres using the force-field parameters reported by Tummala et al.[30] The force-field parameters for bonded interactions of carbon atoms in graphene, including the bond stretching, bond angle, and dihedral potentials, were reported by Patra et al.[31] The water molecules were simulated using the standard SPC/E model.[32] The bond lengths for water molecules during the simulations were constrained using the SETTLE algorithm.[33] The force fields for NMP and GBL were reported by Aparicio et al.[34,35] and are based on OPLS-AA force fields combined with partial charges obtained from quantum-chemical calculations with B3LYP/6-311++G** basis sets using the Gaussian 03 software package.[36] We followed

(14) Blake, P.; Brimicombe, P. D.; Nair, R. R.; Booth, T. J.; Jiang, D.; Schedin, F.; Ponomarenko, L. A.; Morozov, S. V.; Gleeson, H. F.; Hill, E. W.; Geim, A. K.; Novoselov, K. S. *Nano Lett.* **2008**, *8*, 1704–1708.
(15) Hernandez, Y.; et al. *Nat. Nanotechnol.* **2008**, *3*, 563–568.
(16) Lotya, M.; Hernandez, Y.; King, P. J.; Smith, R. J.; Nicolosi, V.; Karlsson, L. S.; Blighe, F. M.; De, S.; Wang, Z. M.; McGovern, I. T.; Duesberg, G. S.; Coleman, J. N. *J. Am. Chem. Soc.* **2009**, *131*, 3611–3620.
(17) Hamilton, C. E.; Lomeda, J. R.; Sun, Z. Z.; Tour, J. M.; Barron, A. R. *Nano Lett.* **2009**, *9*, 3460–3462.
(18) An, X.; Simmons, T.; Shah, R.; Wolfe, C.; Lewis, K. M.; Washington, M.; Nayak, S. K.; Talapatra, S.; Kar, S. *Nano Lett.* [Online early access]. DOI: 10.1021/nl903557p. Published Online: June 17, 2010.
(19) Green, A. A.; Hersam, M. C. *J. Phys. Chem. Lett.* **2010**, *1*, 544–549.
(20) Enoki, T.; Suzuki, M.; Endo, M. *Graphite Intercalation Compounds and Applications*; Oxford University Press: New York, 2003.
(21) Valles, C.; Drummond, C.; Saadaoui, H.; Furtado, C. A.; He, M.; Roubeau, O.; Ortolani, L.; Monthioux, M.; Penicaud, A. *J. Am. Chem. Soc.* **2008**, *130*, 15802–15804.
(22) Ang, P. K.; Wang, S. A.; Bao, Q. L.; Thong, J. T. L.; Loh, K. P. *ACS Nano* **2009**, *3*, 3587–3594.
(23) Sun, Z. Y.; O'Connor, I.; Bergin, S. D.; Coleman, J. N. *J. Phys. Chem. C* **2009**, *113*, 1260–1266.
(24) Hernandez, Y.; Lotya, M.; Rickard, D.; Bergin, S. D.; Coleman, J. N. *Langmuir* **2010**, *26*, 3208–3213.
(25) Konatham, D.; Striolo, A. *Nano Lett.* **2008**, *8*, 4630–4641.
(26) Hummer, G.; Rasaiah, J. C.; Noworyta, J. P. *Nature* **2001**, *414*, 188–190.
(27) Choudhury, N.; Pettitt, B. M. *J. Am. Chem. Soc.* **2005**, *127*, 3556–3567.
(28) Van der Spoel, D.; Lindahl, E.; Hess, B.; Groenhof, G.; Mark, A. E.; Berendsen, H. J. C. *J. Comput. Chem.* **2005**, *26*, 1701–1718.
(29) Jorgensen, W. L.; Maxwell, D. S.; Tirado-Rives, J. *J. Am. Chem. Soc.* **1996**, *118*, 11225–11236.
(30) Tummala, N. R.; Striolo, A. *J. Phys. Chem. B* **2008**, *112*, 1987–2000.
(31) Patra, N.; Wang, B. Y.; Kral, P. *Nano Lett.* **2009**, *9*, 3766–3771.
(32) Berendsen, H. J. C.; Grigera, J. R.; Straatsma, T. P. *J. Phys. Chem.* **1987**, *91*, 6269–6271.
(33) Miyamoto, S.; Kollman, P. A. *J. Comput. Chem.* **1992**, *13*, 952–962.
(34) Aparicio, S.; Alcalde, R.; Davila, M. J.; Garcia, B.; Leal, J. M. *J. Phys. Chem. B* **2008**, *112*, 11361–11373.
(35) Aparicio, S.; Alcalde, R. *Phys. Chem. Chem. Phys.* **2009**, *11*, 6455–6467.
(36) Curtiss, L. A.; Redfern, P. C.; Raghavachari, K.; Pople, J. A. *Chem. Phys. Lett.* **2002**, *359*, 390–396.

Table 1. Comparison of the MD-Simulated and Experimental Bulk Densities of the Five Solvents Considered at 1.0 bar and 298.15 K

	water	NMP	DMF	GBL	DMSO
MD-simulated density (g/L)	999.3	1032.6	941.6	1121.5	1092.0
experimental density (g/L)[40]	997	1028	944	1129	1100

the same procedures to develop new force fields for DMF, and we used the existing OPLS-AA force field for DMSO. The partial charges of each atom in DMF and DMSO used in our MD simulations are reported in Table S1 in the Supporting Information. Bond lengths in the solvent molecules were constrained using the parallel version of the LINCS algorithm.[37,38] The vdW interactions were treated with a cutoff distance of 0.9 nm. The vdW attractions and steric repulsions between different atoms were calculated from the LJ potential using the standard geometric averaging rule as implemented in the OPLS-AA force field.[22] Long-range electrostatic interactions were treated using the particle-mesh Ewald (PME) summation method.[39,40]

The equations of motion were integrated with a time step of 2 fs using the Verlet (leapfrog) algorithm.[41,42] The velocity-rescaled Berendsen thermostat was implemented to maintain the system at a constant temperature.[43] The pressure was coupled to an isotropic Berendsen barostat.[44] Periodic boundary conditions were applied in all three directions. The trajectories, velocities, and forces corresponding to all the atoms in the system were saved every 10 000 steps (20 ps) to satisfy the ergodicity criterion for data analysis.[45] Comparison of our MD-simulated average bulk densities with the experimental values[46] for the five solvents considered showed that the differences are smaller than 1% (see Table 1).

To investigate the interactions between two parallel graphene sheets in each solvent, we calculated the PMF by numerically integrating (with the trapezoidal method) the interaction forces required to separate the two parallel and fixed graphene sheets at various intersheet separations.[47,48] This integration process started at the largest intersheet separation (15 Å), at which the PMF was set to be zero, and ended at the smallest intersheet separation simulated (3.2 Å). The initial configurations were generated by placing the two parallel graphene sheets at different intersheet separations and then filling the simulation box with a sufficient number of randomized solvent molecules. Since the interaction between two parallel graphene sheets requires 1−3 ns to reach equilibrium, each simulated system was equilibrated for 10 ns. For the systems simulated at various intersheet separations, only the last 5 ns of each simulation was used for data analysis, including the PMF calculations.

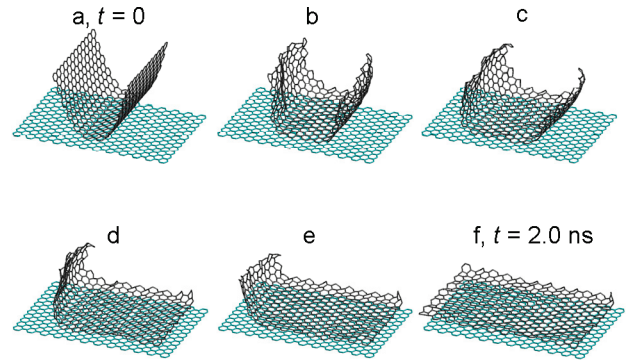

Figure 1. MD simulation of two partially exfoliated single-layer graphene sheets in NMP solvent as a function of simulation time. The smallest intersheet separation at all times was 3.5 Å.

3. Results and Discussion

3.1. Interactions between Graphene Sheets and Solvent Molecules. First, we discuss the role of the solvent in solvating and exfoliating graphene sheets. To this end, we considered two partially exfoliated graphene sheets (area = 49.7 Å × 29.5 Å) solvated in NMP at $t = 0$, as shown in Figure 1. It should be recalled that in experiments the gap between graphene sheets can form as a result of several micromechanical processes, including ultrasonication or strong agitation.[49] Also, it should be noted that the planar graphene sheet shown in Figure 1 was fixed in order to more easily monitor the simulated exfoliation process. The two partially exfoliated sheets at $t = 0$ recombined spontaneously within 2.0 ns, forming AB-stacked bilayer graphene. The implication of the finding in Figure 1 is that the graphene−NMP interaction is not sufficiently strong to completely overcome the intergraphene vdW interaction. Alternatively, one may conclude that the affinity of the NMP molecules for graphene is not sufficiently strong for NMP to wet the graphene surface, and therefore, the NMP molecules are not able to intercalate between the two graphene sheets. In summary, NMP molecules by themselves cannot exfoliate graphene.

Next, MD simulations of two large, parallel single-layer graphene sheets (area = 73.8 Å × 76.7 Å) solvated in a 10 nm × 10 nm × 8 nm NMP box were carried out to investigate the interactions of graphene sheets through NMP. By variation of the separation between the two sheets, d, the PMF was calculated through numerical integration of the d-dependent interaction force between the two sheets with respect to d (see the red curve in Figure 2b).[47] The blue curve in Figure 2b shows the time-averaged number of NMP molecules confined between the two graphene sheets as a function of d. In addition, to visualize the structural arrangement of the NMP molecules near the two graphene sheets, Figure 2a shows the organization of the NMP molecules as a function of d. Finally, Figure 2c shows ρ/ρ_{bulk}, the normalized density profile of NMP along the z axis (i.e., normal to the sheet surface), corresponding to each of the points a−f on the blue curve in Figure 2b. In panels a−f in Figure 2c, the observed large NMP density peaks outside the two sheets (facing the bulk), indicating significant layering of the NMP molecules in the two adjacent outer solvent regions. As d is reduced from 10 Å in a to 6.4 Å in f, the confined NMP molecules successively form four-layer (at d = 10 Å), two-layer (at d = 9.2 Å), and single-layer (6.6 Å < d < 8.4 Å)

(37) Hess, B.; Bekker, H.; Berendsen, H. J. C.; Fraaije, J. G. E. M. *J. Comput. Chem.* **1997**, *18*, 1463–1472.
(38) Hess, B. *J. Chem. Theory Comput.* **2008**, *4*, 116–122.
(39) Darden, T.; York, D.; Pedersen, L. *J. Chem. Phys.* **1993**, *98*, 10089–10092.
(40) Essmann, U.; Perera, L.; Berkowitz, M. L.; Darden, T.; Lee, H.; Pedersen, L. G. *J. Chem. Phys.* **1995**, *103*, 8577–8593.
(41) Hockney, R. W.; Goel, S. P.; Eastwood, J. W. *J. Comput. Phys.* **1974**, *14*, 148–158.
(42) Verlet, L. *Phys. Rev.* **1967**, *159*, 98–101.
(43) Bussi, G.; Donadio, D.; Parrinello, M. *J. Chem. Phys.* **2007**, *126*, 014101.
(44) Berendsen, H. J. C.; Postma, J. P. M.; Van Gunsteren, W. F.; Dinola, A.; Haak, J. R. *J. Chem. Phys.* **1984**, *81*, 3684–3690.
(45) Leach, A. R. *Molecular Modelling: Principles and Applications*, 2nd ed.; Prentice Hall: Upper Saddle River, NJ, 2001.
(46) Lide, D. R.; CRC Press. In *CRC Press Database*, version 2.0; CRC Press: Boca Raton, FL, 1996.
(47) Xu, Z. J.; Yang, X. N.; Yang, Z. *Nano Lett.* **2010**, *10*, 985–991.
(48) Uddin, N. M.; Capaldi, F.; Farouk, B. *J. Eng. Mater. Technol.* **2010**, *132*, 021012.
(49) Strano, M. S.; Moore, V. C.; Miller, M. K.; Allen, M. J.; Haroz, E. H.; Kittrell, C.; Hauge, R. H.; Smalley, R. E. *J. Nanosci. Nanotechnol.* **2003**, *3*, 81–86.

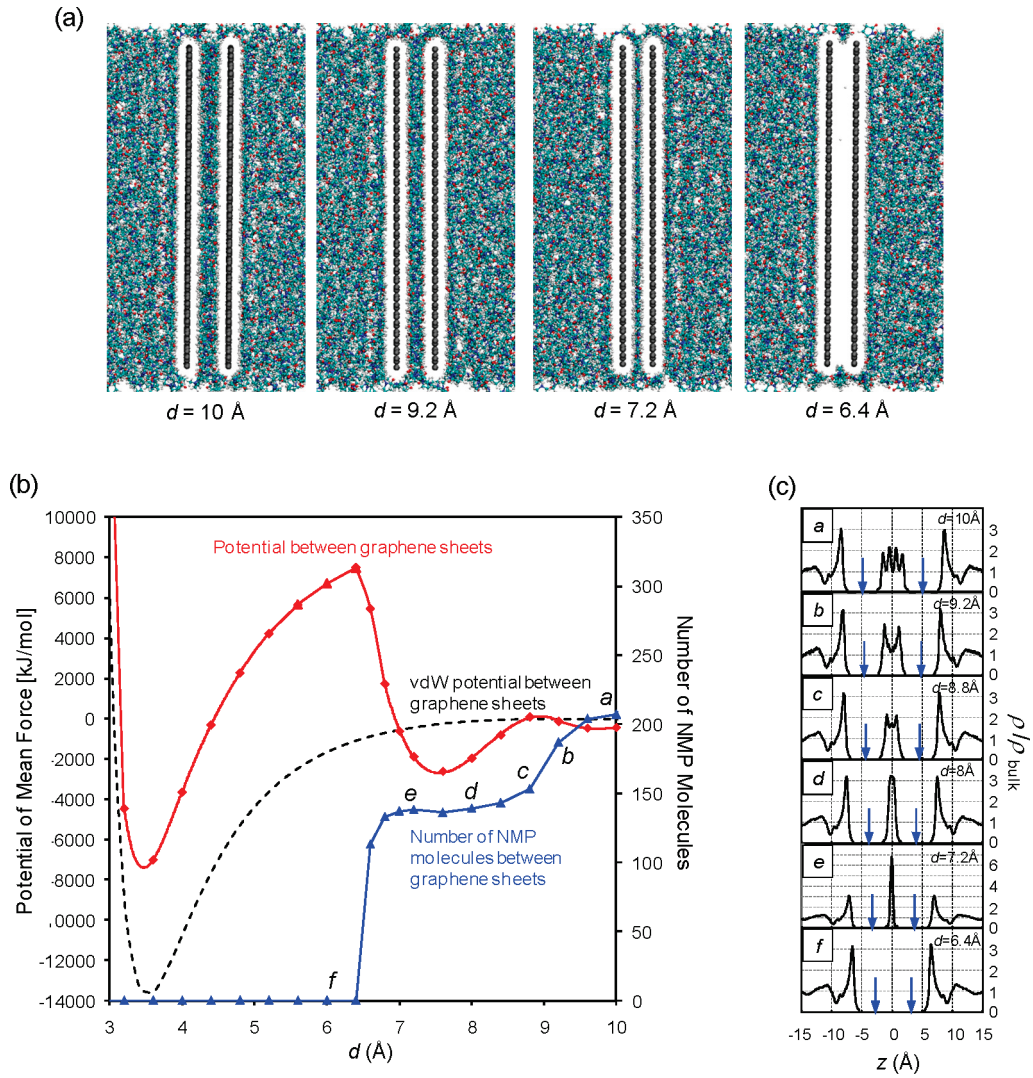

Figure 2. Simulated potential of mean force between two parallel single-layer graphene sheets in NMP solvent. (a) Representative configurations of the graphene sheets and NMP molecules at various intersheet separations d. (b) Potential of mean force between two graphene sheets (red curve), number of confined NMP molecules between the two graphene sheets (blue curve), and LJ interaction potential between the two graphene sheets in the absence of NMP molecules (dashed curve) as functions of d. (c) Normalized density profiles of NMP, ρ/ρ_{bulk}, as functions of the z coordinate used in the MD simulations (perpendicular to the graphene sheet surface) corresponding to points $a-f$ in (b). The blue arrows in (c) denote the locations of the two graphene sheets.

structures, after which an NMP-depleted region is formed for $d < 6.6$ Å. For $d > 8.4$ Å, the number of confined NMP molecules decreases gradually with decreasing d; the four-layer and two-layer structures do not appear to be very stable, since they can be altered by slight changes in the confinement volume. The variation in the confined NMP layering and density at the surface of the graphene sheets results in oscillatory interaction forces between the two sheets.[50,51] This in turn leads to the small oscillations observed in the PMF curve for $d > 8.4$ Å (see Figure 2b). However, these oscillations for $d > 8.4$ Å are negligible relative to the variations in the PMF curve resulting from the last confined NMP layer (for 6.6 Å $< d <$ 8.4 Å). Indeed, the single-layer NMP molecules exhibit very different behavior. As shown in Figure 2b, the number of confined NMP molecules (the blue curve) remains reasonably constant for 6.8 Å $< d <$ 8.4 Å, and the associated PMF curve exhibits an asymmetric parabolic behavior with a minimum at $d \approx 7.6$ Å. For 6.6 Å $< d < 7.6$ Å, the PMF increases sharply and reaches a maximum at $d = 6.6$ Å. This energy barrier corresponds to the energy required to desorb the confined single layer of NMP molecules. Since the interaction force is equal to the negative of the derivative of the PMF with respect to d (so an attractive force is a negative in sign while a repulsive force is positive in sign), it follows that the interaction force between the two graphene sheets changes from attractive (for 7.6 Å $< d <$ 8.4 Å) to highly repulsive (for 6.6 Å $\leq d <$ 7.6 Å). This indicates that the single layer of NMP molecules has a very strong affinity for the graphene sheets and therefore is thermodynamically favored to be confined between the sheets for 6.6 Å $\leq d <$ 7.6 Å. We will examine the physical origin of the interaction potential in more detail later. As shown in the red PMF curve in Figure 2b, the major barrier preventing the graphene sheets from undergoing aggregation corresponds to desorption of the last layer of confined NMP molecules (see e and f in Figure 2c).

As stressed above, upon further reduction of the confinement distance ($d < 6.6$ Å), the dramatic increase in the interaction potential between graphene and the NMP molecules destabilizes

(50) Snook, I.; Megen, W. V. *J. Chem. Phys.* **1979**, *70*, 3099–3105.
(51) Israelachvili, J. N. *Intermolecular and Surface Forces*; Academic Press: London, 1985.

the single layer of NMP molecules, which in turn leads to desorption of the confined NMP molecules. This behavior is related to the steric hindrance discussed by Choudhury and Pettitt.[27] Since no NMP molecules reside between the two graphene sheets for $d < 6.6$ Å, the intersheet vdW interaction potential dominates, and the PMF curve decreases rapidly until d is equal to the interlayer separation of graphite, $r_0 \approx 3.5$ Å (see the red curve in Figure 2b). It should be noted that because we considered two parallel graphene sheets, r_0 is equal to the distance between two AA-stacked graphite layers, which is 3.5 Å. A further reduction in d to values less than r_0 results in a dramatic increase in the PMF curve, as described by the well-known repulsive contribution to the Lennard-Jones (LJ) potential.[52] For comparison purposes, the simulated LJ interaction potential between two parallel graphene sheets in vacuum is shown as the dashed curve in Figure 2b. Comparison of the red PMF curve and the dashed PMF curve clearly shows that the NMP molecules can stabilize the two graphene sheets by both providing a high energy barrier and decreasing the depth of the interlayer vdW well. From the perspective of the kinetics of colloid aggregation (i.e., the graphene → graphite recombination reaction), a higher energy barrier results in a smaller aggregation rate, while a shallower vdW well results in a larger equilibrium concentration of graphene sheets.[53] As we will show below, combining the PMF obtained from the MD simulations with the kinetic theory of colloid aggregation enables the stability of graphene in NMP and other solvents to be quantified.

In the theoretical approach presented here, in order to model the kinetics of graphene aggregation in a solvent, the first step involves modeling the PMF curve. Since we were considering highly polar solvents confined between two graphene sheets, the approximations used in the past to model liquids confined between two mica surfaces as ensembles of spherelike or chainlike particles[51,54] could not adequately describe the unique features associated with the PMF in the present case. As discussed above, our MD simulations showed that the last confined liquid layer dominates the behavior of the PMF (see Figure 2b). Accordingly, we propose the following semiempirical analytical model to describe the potential of mean force per unit area, Φ, between two parallel graphene sheets separated by a distance d:

$$\Phi = \varepsilon\left[\left(\frac{r_0}{d}\right)^{12} - 2\left(\frac{r_0}{d}\right)^{6}\right] + \beta_1 \exp\left(\frac{-(d - r_1)^2}{2\sigma_1^2}\right) - \beta_2 \exp\left(\frac{-(d - r_2)^2}{2\sigma_2^2}\right) \quad (1)$$

where ε and r_0 are the well-known parameters in the LJ potential; β_1, r_1, and σ_1 characterize the height, location, and width, respectively, of the energy barrier; and β_2, r_2, and σ_2 characterize the depth, location, and width, respectively, of the secondary energy well (see Figure 3). The parameters in eq 1 can be obtained by least-squares fitting of eq 1 to the PMF curve obtained using the MD simulations. It should be noted that eq 1 physically captures only the effect of the last confined layer of solvent molecules and neglects other small oscillations associated with changes of confined multilayer solvent structures.

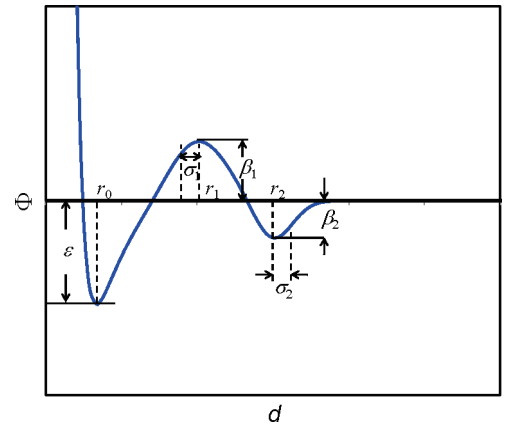

Figure 3. Schematic representation of the semiempirical model (eq 1) used to describe the potential of mean force per unit area, Φ, between two parallel graphene sheets as a function of the intersheet separation d.

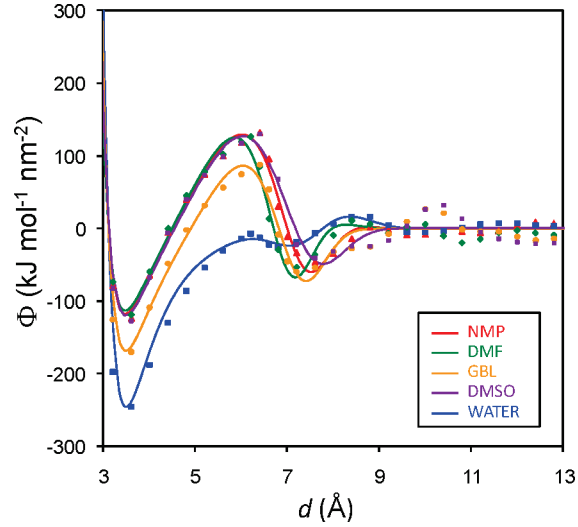

Figure 4. Potentials of mean force per unit area, Φ, between two parallel graphene sheets in the five solvents considered here (NMP, DMF, GBL, DMSO, and water) as functions of the intersheet separation d, as calculated using MD simulations (symbols) and least-squares fitting of eq 1 (solid curves).

In addition to NMP, large-scale MD simulations were carried out to calculate the PMFs corresponding to four other common solvents used to disperse graphene: DMF, GBL, DMSO, and water. Using the PMF model in eq 1, we were able to fit the simulated PMF curves of the five solvents reasonably well, as shown in Figure 4. The corresponding fitted values of the parameters in eq 1 for the five solvents are reported in Table S2 in the Supporting Information. Because the effect of the last confined layer of solvent molecules dominates over those of other layers of solvent molecules and typically comes into play when $d < 9$ Å, we fitted the PMF data points only over this size range in order to capture the main features of the PMF curve. In addition, we left the fitted line flat at a value of zero beyond this range (see Figure 4) to avoid possible numerical errors. Among the five solvents, water clearly shows the lowest energy barrier and the deepest interlayer vdW well and therefore should be the least efficient solvent in stabilizing graphene. This finding clearly explains the observation that during the reduction process of graphene oxide in water, when the oxygen functionality is removed to yield graphene, the graphene sheets lose their dispersibility, aggregate, and finally precipitate during a

(52) Lennard-Jones, J. E. *Proc. R. Soc. London, Ser. A* **1925**, *109*, 584–597.
(53) Hiemenz, P. C.; Rajagopalan, R. *Principles of Colloid and Surface Chemistry*, 3rd ed.; Marcel Dekker: New York, 1997.
(54) Tarazona, P.; Vicente, L. *Mol. Phys.* **1985**, *56*, 557–572.

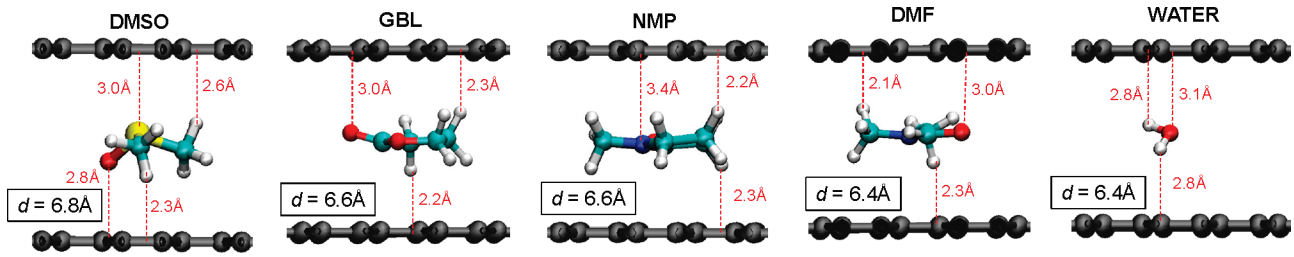

Figure 5. Simulated representative configurations of the five considered types of solvent molecules between two parallel single-layer graphene sheets at the corresponding most confined intersheet separations d (i.e., the smallest d values at which single-layer solvent molecules can exist between the two graphene sheets in a stable manner). Each sphere represents an atom using the following color scheme: white, H; green, solvent-molecule C; red, O; blue, N; yellow, S; black, graphene C.

Table 2. Interatomic Distances r_{min} at the Minima of the LJ Potentials Corresponding to the Atomic Pairs Considered in Our MD Simulations (C Denotes Carbon Atoms in the Graphene Sheets)

atomic pair	C−H	C−O	C−S	C−N
r_{min} (Å)	3.3	3.7	3.9	3.7

very short time.[55] Pure water is not capable of dispersing graphene in a stable manner unless one adds suitable amphiphilic molecules.[16,18] The other four solvents, GBL, NMP, DMF, and DMSO, are significantly more efficient at stabilizing graphene by providing higher energy barriers and shallower vdW wells (see Figure 4).

Since the height of the energy barrier controls the stability of graphene in a solvent, the following questions can be asked about the last single layer of confined solvent molecules: (i) What is the origin of the highly repulsive force between the graphene sheets? (ii) Why do the solvent molecules prefer to be confined even when the repulsive force operates? (iii) What is the criterion for formation of a stable single layer of confined solvent molecules? To answer these questions, simulated cross-sectional views of the most confined solvent molecules between two parallel graphene sheets (i.e., one confined at the smallest d value at which single-layer solvent molecules can exist between the two sheets in a stable manner) for the five solvents considered are shown in Figure 5. Because of the nonpolar nature of the graphene sheets, interactions between graphene and the confined polar solvent molecules can be described by the LJ potential. Therefore, the overall interaction potential between graphene and the polar solvent is equal to the sum of all of the LJ potentials between individual atoms in the solvent molecules and in graphene. Table 2 gives values of r_{min}, the interatomic distance at the minimum of the LJ potential corresponding to each atomic pair considered in our MD simulations. For the four most efficient graphene-stabilizing solvents studied (NMP, DMF, GBL, and DMSO), comparison of the various r_{min} values with the simulated atomic distances between solvent and graphene atoms (see Figure 5) clearly shows that the highly repulsive interaction results from the sharp increase in the steric repulsive contribution[52] to the LJ potential at short range. This is due to the fact that the various interatomic vdW bond lengths are smaller than their corresponding r_{min} values. For NMP and DMF, the repulsive interaction results from the compression of the C−H, C−O, and C−N vdW bonds vertical to the graphene sheet surface, where C refers to the carbon atoms of graphene. For GBL, the repulsive interaction results from the compression of the C−H and C−O vdW bonds vertical to the graphene sheet surface. For DMSO, the repulsive interaction results from the compression of the C−H, C−O, and C−S vdW bonds vertical to the graphene sheet surface. Again, water displays a very different behavior, as the C−H and C−O vdW bonds are all only slightly smaller than their r_{min} values. As a result, even a slight increase in the LJ potential resulting from a further reduction in d should expel all of the confined water molecules, giving a PMF barrier height of almost zero for water.

When the solvent molecules are confined in a single-layer structure, they apparently lose some of the solvent−solvent interaction energy because of a reduction in the number of adjacent solvent molecules. Since the calculated interaction energies are negative, this loss results in an increase in the potential energy relative to that of the bulk solvent phase. Furthermore, the interaction energy between graphene and solvent molecules is also negative. Under these conditions, the solvent molecules still favor being confined because the negative solvent−graphene interaction energy compensates for the increase in solvent−solvent interaction energy. However, compression of the vdW bonds between graphene and the solvent molecules results in an increase in the potential energy of the confined solvent molecules. Once the increase in the solvent−graphene interaction energy due to the compression effect becomes large enough that the total potential energy of the confined solvent molecules exceeds the bulk solvent−solvent potential energy, the confined solvent molecules desorb, and the two graphene sheets can then overcome the energy barrier. To quantify this behavior, it is useful to consider the simulated potential energy difference between one mole of confined single-layer solvent molecules and one mole of solvent molecules in the bulk, $\Delta U = U_{confined} - U_{bulk}$, as a function of d. Figure 6a shows the simulated ΔU-versus-d profiles for the five solvents considered. The error bars correspond to the standard deviations of the energy fluctuations of confined solvent molecules at specific intersheet separations. Because the number of confined solvent molecules does not change appreciably with d (for 6.6 Å < d < 8.4 Å in the NMP case, as shown in Figure 2b), the observed variations in ΔU as a function of d can be attributed mainly to the interactions between the solvent molecules and graphene. Consequently, the behavior of ΔU versus d exhibits features that are very similar to those exhibited by the LJ potential. Specifically, at the onset of the formation of a single layer of confined solvent molecules (at $d \approx 8$ Å for the five solvents considered), $U_{confined}$ is only slightly lower than U_{bulk} because the distance between graphene and the solvent molecules is relatively large, so the interactions between the solvent molecules and graphene are not very strong. As the intersheet separation decreases, ΔU decreases and then increases sharply.

(55) Si, Y.; Samulski, E. T. *Nano Lett.* **2008**, *8*, 1679–1682.

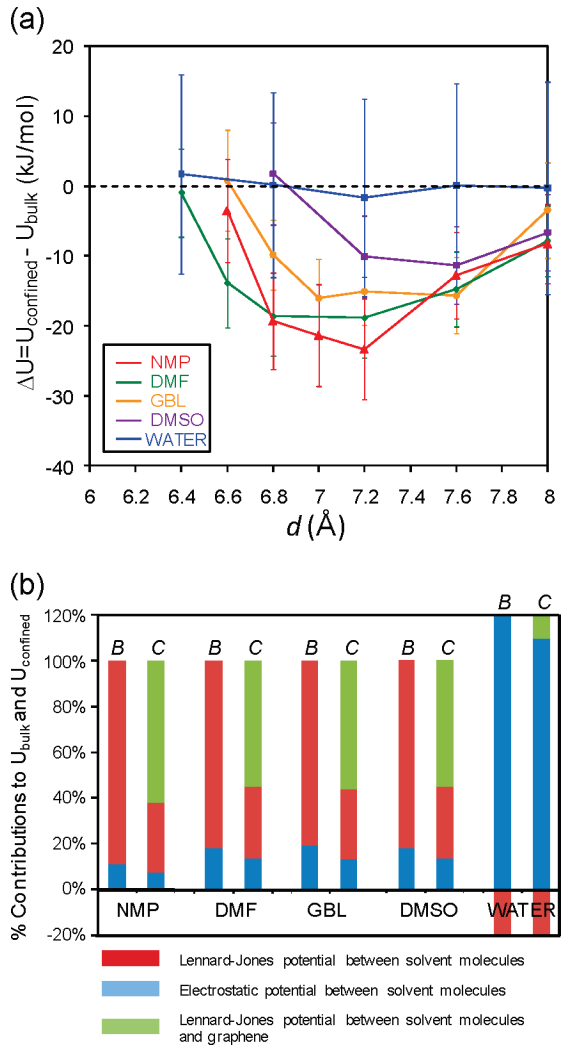

Figure 6. (a) Simulated values of $\Delta U = U_{confined} - U_{bulk}$, the difference between the potential energies of one mole of confined solvent molecules located between two parallel graphene sheets ($U_{confined}$) and one mole of solvent molecules in the bulk phase (U_{bulk}), as a function of intersheet separation d for the five solvents considered. The error bars correspond to the standard deviations of the energy fluctuations of confined solvent molecules at specific intersheet separations. (b) Simulated percent contributions to the potential energy from the bulk (B) and most confined (C) solvent molecules (the configuration corresponding to the smallest d value at which the single-layer solvent molecules can exist between two parallel graphene sheets in a stable manner) for the five solvents considered. The red bar corresponds to the contribution from the Lennard-Jones potential between the solvent molecules, the blue bar to the electrostatic (dipole−dipole) potential between the solvent molecules, and the green bar to the contribution from the Lennard-Jones potential between the solvent molecules and the two graphene sheets.

The minimum shown in Figure 6a for each solvent corresponds to the minimum in the sum of the LJ potentials between each atom in a given solvent and graphene. At the specific intersheet separation d_{min}, the interactions between the solvent molecules and graphene are the strongest for each solvent. For the NMP solvent, d_{min} is very close to the separation corresponding to the minimum of the secondary energy well ($d = 7.6$ Å) that we reported in Figure 2b. The observed increase in ΔU as d decreases below d_{min} results from the compression of the vdW bonds, as discussed earlier. Intersheet separations that are too compressed result in $\Delta U > 0$ (i.e., $U_{confined} > U_{bulk}$), so the confined single-layer solvent structure destabilizes and desorbs from the gap. Therefore, the most confined solvent molecules (simulated $d = 6.6$ Å for the NMP solvent case; see Figures 5 and 6a) correspond to $U_{confined} \approx U_{bulk}$, or $\Delta U = 0$. As shown in Figure 6a, in terms of efficient solvents (NMP, DMF, DMSO, and GBL), the solvent−graphene interactions can provide between −10 and −20 kJ/mol more interaction energy (as reflected in the depth of the ΔU well) to stabilize the confined single layer of solvent molecules. This potential energy difference can offset the range of energy increases resulting from the compression of interatomic vdW bonds between graphene and the solvent molecules. As a result, the simulated vdW bond lengths can be smaller than their corresponding r_{min} values (see Figure 5).

Figure 6b shows the percent contributions to the potential energy from the most confined (at the separation d corresponding to Figure 5) solvent molecules, $U_{confined}$, and the bulk solvent molecules, U_{bulk}, for the five solvents considered. For the most efficient solvents (NMP, DMF, GBL, and DMSO), although they are highly polar in the bulk solvent phase (B) (e.g., the dipole moment of an NMP molecule is 4.2 D), the LJ potential between the solvent molecules (the red bar) still dominates their contribution to U_{bulk} (up to 80%), while the remaining 20% results from the electrostatic (dipole−dipole) contribution (the blue bar). Surprisingly, for the most confined single-layer solvent molecules (C), the graphene−solvent LJ potential (the green bar) contributes up to 60% of the potential energy loss because of the reduction in the number of adjacent solvent molecules. However, in comparison with the four efficient solvents considered, water shows very different behavior, as depicted in the last two bars in Figure 6b. In the bulk water phase (B), strong hydrogen bonds, which are described by an electrostatic potential (the blue bar), result in an intermolecular separation between water molecules (2.7 Å on average) that is smaller than the r_{min} value corresponding the O−O vdW bond length (3.6 Å). As a result, the water−water LJ potential (the red bar) is positive (it should be noted that because the total potential energy is negative, the percent contribution from the water−water LJ potential is negative and the sum of other contributions exceeds 100%). Since strong hydrogen bonding dominates the water intermolecular potential and the size of a water molecule is small, the water−graphene LJ potential (the green bar) can contribute only 10% of the potential energy of the confined water molecules (C). This weak interaction is in fact the molecular origin of the hydrophobicity of graphene. As shown in Figure 6a, for water, $\Delta U \approx 0$ at all values of d, and therefore, a slight increase in the graphene−water potential energy due to the compression of the two parallel graphene sheets destabilizes the confined water layer, as discussed earlier.

We can therefore conclude that the stronger affinity of the solvent molecules for graphene than for themselves plays the key role in imparting more negative potential energies to the confined solvent molecules. On the basis of our findings, a promising strategy for molecular design of a more efficient graphene-stabilizing solvent may involve tuning its chemical structure and atomic arrangement to make the minimum in the ΔU-versus-d profile as deep as possible.

3.2. Kinetics of Graphene Aggregation. The theoretical analysis presented so far has provided a thermodynamic description of the stability of graphene in various polar solvents. However, for practical purposes, the kinetics of graphene sheet aggregation must be investigated to correlate the simulated PMF results with the time-dependent graphene layer distribution observed in actual experiments. With this in mind, we next present a theoretical model that combines the PMF results from

our MD simulations with the theory of slow colloid coagulation[56] and allows a rational selection of efficient solvents for stabilizing graphene dispersions.

Individually suspended graphene sheets in a solvent can translate and rotate freely because of their kinetic energy. As a result, these micrometer-sized particles may be modeled as effective spheres. Initially, we will assume that the aggregation process is diffusion-controlled, and subsequently, we will introduce interaction effects. The derivation presented below is based on the diffusion of single-layer graphene sheets toward a stationary *i*-layer graphene sheet. The diffusion (Brownian motion) of graphene sheets can be described by Fick's first law. Specifically, the diffusive flux J_{1i}^{diff} as a function of the radial distance r from the reference *i*-layer graphene sheet is given by[56]

$$J_{1i}^{\text{diff}}(r) = -D_1 \frac{\mathrm{d}N_1}{\mathrm{d}r} \tag{2}$$

where J_{1i}^{diff} is the number of single-layer graphene sheets approaching the reference *i*-layer graphene sheet per unit area per unit time in the absence of intercolloid interactions, N_1 is the number of single-layer graphene sheets per unit volume (i.e., the concentration), and D_1 is the diffusivity of a single-layer graphene sheet in the solvent.

To account for the effect of intercolloid interactions, we next include the flux resulting from $V_{1i}(r)$, the intercolloid interaction potential energy between the single-layer and *i*-layer graphene sheets. Associated with the interaction potential $V_{1i}(r)$, a force $F_{1i} = -(\mathrm{d}V_{1i}/\mathrm{d}r)$ operates between the graphene layers, resulting in an effective drift velocity v_{1i}^{eff} of the diffusing single-layer graphene sheets:

$$F_{1i} = -\frac{\mathrm{d}V_{1i}}{\mathrm{d}r} = v_{1i}^{\text{eff}} f_1$$

where f_1 is the friction factor of single-layer graphene. Thus, v_{1i}^{eff} is given by

$$v_{1i}^{\text{eff}} = -\frac{1}{f_1}\frac{\mathrm{d}V_{1i}}{\mathrm{d}r} \tag{3}$$

According to the Stokes−Einstein relation,[56] it follows that

$$f_1 = \frac{k_{\text{B}}T}{D_1} \tag{4}$$

where k_{B} is the Boltzmann constant and T is the absolute temperature.

The diffusive flux J_{1i}^{diff} in eq 2 can now be modified to include the drift flux J_{1i}^{eff}, which is equal to $N_1 v_{1i}^{\text{eff}}$. Specifically, the total flux $J_{1i}(r)$ is given by:

$$\begin{aligned} J_{1i}(r) &= J_{1i}^{\text{eff}} + J_{1i}^{\text{diff}} \\ &= -D_1\frac{\mathrm{d}N_1}{\mathrm{d}r} + N_1 v_{1i}^{\text{eff}} \\ &= -D_1\left[\frac{\mathrm{d}N_1}{\mathrm{d}r} + N_1\frac{\mathrm{d}(V_{1i}/k_{\text{B}}T)}{\mathrm{d}r}\right] \end{aligned} \tag{5}$$

where we have used eqs 3 and 4. Since the flux is positive in the positive radial direction, the number of single-layer graphene sheets transported toward the spherical cross section of area $4\pi r^2$ around the central *i*-layer graphene sheet per unit time corresponds to the collision frequency of single-layer graphene sheets toward an *i*-layer graphene sheet, Z_{1i}, which is given by

$$Z_{1i} = -4\pi r^2 J_{1i} = 4\pi D_1 r^2\left[\frac{\mathrm{d}N_1}{\mathrm{d}r} + N_1\frac{\mathrm{d}(V_{1i}/k_{\text{B}}T)}{\mathrm{d}r}\right] \tag{6}$$

where eq 5 was used.

At steady state, the collision frequency between graphene sheets that results in aggregation, Z_{1i}, is constant because there are no homogeneous reactions (it should be noted that the term "collision" used here refers to a collision between graphene sheets that results in aggregation). Equation 6 can be simplified by introducing the variable $y(r)$ as follows:

$$y(r) = N_1(r)\exp[V_{1i}(r)/k_{\text{B}}T] \tag{7}$$

Using eq 7, we can simplify eq 6 as follows:

$$\mathrm{d}y = \frac{Z_{1i}}{4\pi D_1}\frac{\exp[V_{1i}(r)/k_{\text{B}}T]}{r^2}\,\mathrm{d}r \tag{8}$$

Since Z_{1i} and D_1 are constants, eq 8 can be integrated from r to $r = \infty$, where $V_{1i} = 0$ and $N_1 = N_{\text{b}1}$ (the bulk concentration of single-layer graphene). Specifically, we obtain

$$\begin{aligned} y(\infty) - y(r) &= N_{\text{b}1} - N_1(r)\exp[V_{1i}(r)/k_{\text{B}}T] \\ &= \frac{Z_{1i}}{4\pi D_1}\int_r^\infty \frac{\exp(V_{1i}/k_{\text{B}}T)}{r^2}\,\mathrm{d}r \end{aligned} \tag{9}$$

Rearranging eq 9 yields

$$N_1(r) = \exp[-V_{1i}(r)/k_{\text{B}}T] \times \left[N_{\text{b}1} - \frac{Z_{1i}}{4\pi D_1}\int_r^\infty \frac{\exp(V_{1i}/k_{\text{B}}T)}{r^2}\,\mathrm{d}r\right] \tag{10}$$

The collision frequency Z_{1i} can be calculated by recognizing that when a single-layer graphene sheet and an *i*-layer graphene sheet are at the distance of closest approach, $r = r_0 = 3.5$ Å, they recombine, or react, to form an $(i + 1)$-layer graphene sheet. As a result, it follows that $N_1(r = r_0) = 0$. Using this in eq 10 and solving for the collision frequency Z_{1i}, we find that

$$Z_{1i} = \frac{4\pi D_1 N_{\text{b}1}}{\displaystyle\int_{r_0}^\infty \frac{\exp[V_{1i}(r)/k_{\text{B}}T]}{r^2}\,\mathrm{d}r} \tag{11}$$

The derivation presented above was based on the diffusion of single-layer graphene sheets toward a stationary *i*-layer graphene sheet. For the case of two mutually diffusing graphene sheets, D_1 must be replaced by $D_{1i} = D_1 + D_i$, where D_i is the diffusivity of an *i*-layer graphene sheet. The rate of collision, and hence the reaction rate, of the single-layer graphene sheets is equal to the product of the collision frequency Z_{1i} and the bulk concentration of *i*-layer graphene sheets, $N_{\text{b}i}$. When all possible collisions (reaction pairs) are considered, the total rate of collision is given by

$$\begin{aligned} \frac{\mathrm{d}N_{\text{b}1}}{\mathrm{d}t} &= -\sum_{i=1}^{N_{\max}} Z_{1i}N_{\text{b}i} = -\sum_{i=1}^{N_{\max}} k_{1i}N_{\text{b}1}N_{\text{b}i} \\ &= -\sum_{i=1}^{N_{\max}} \frac{4\pi(D_1 + D_i)}{\displaystyle\int_{r_0}^\infty \frac{\exp(V_{1i}/k_{\text{B}}T)}{r^2}\,\mathrm{d}r} N_{\text{b}1}N_{\text{b}i} \end{aligned} \tag{12}$$

(56) Fuchs, N. *Z. Phys. Chem., Abt. A* **1934**, *171*, 199–208.

where N_{max} is the maximum number of graphene sheet layers that can exist in the solvent phase in a stable manner and k_{1i} is the reaction rate constant for the reaction between the single-layer and i-layer graphene sheets. The reaction rate of m-layer graphene sheets ($m \leq N_{max}$) can be formulated similarly. Specifically,

$$\frac{dN_{bm}}{dt} = \frac{1}{2}\sum_{i=1}^{m-1} k_{i,(m-i)} N_{bi} N_{b(m-i)} - \sum_{i=1}^{N_{max}} k_{i,m} N_{bi} N_{bm} \quad (13)$$

where $k_{i,(m-i)}$ and $k_{i,m}$ are the reaction rate constants for the reactions of i-layer and $(m - i)$-layer sheets and i-layer and m-layer sheets, respectively. The factor of $^1/_2$ in eq 13 avoids counting the same collision twice [i.e., $i/(m - i)$ collisions are the same as $(m - i)/i$ collisions]. Similarly, the reaction rate constant $k_{i,m}$ can be expressed as follows:

$$k_{i,m} = \frac{4\pi(D_i + D_m)}{\int_{r_0}^{\infty} \frac{\exp(V_{im}/k_B T)}{r^2}\, dr} \quad (14)$$

To estimate the time-dependent distribution of graphene sheet layers in the solvent, the following assumptions were made to simplify our current model: (i) The lateral size of all graphene sheets is the same. (ii) The diffusivity of graphene sheets is independent of the number of layers i, since the friction factor in the Stokes−Einstein relation mainly depends on the lateral size of a graphene sheet. (iii) Because micrometer-sized graphene sheets are considered here, the diffusivity of graphene was estimated to be 1×10^{-12} m^2/s using Stokes' law at room temperature for all the solvents considered. (iv) Since no graphene sheets thicker than 10 layers were observed experimentally,[15] when $i > 10$, the graphene sheets aggregate and precipitate (i.e., $N_{max} = 10$). (v) Because of the relatively negligible thickness of the graphene sheets, the intersheet interaction potential energy is independent of the number of layers i and m in the two sheets. It is important to recognize that experimental graphene dispersions may not be defect- or impurity-free and that their lateral sizes and shapes are also not uniform. However, taking into account the effects of graphene size and defects would have greatly increased the complexity of the model, whereas the model developed here using the above assumptions allowed us to combine the MD simulations with experimental data in a constructive manner in order to make the many useful qualitative predictions presented in this paper. In the future, we plan to investigate more complex theoretical models that may allow us to quantitatively predict various features associated with the coagulation of graphene in a liquid phase.

On the basis of assumptions (i)−(v), eq 14 can be simplified as follows:

$$k_{i,m} = k = \frac{8\pi D}{\int_{r_0}^{\infty} \frac{\exp(V/k_B T)}{r^2}\, dr} \quad (15)$$

It is noteworthy that when two graphene sheets approach, all collision angles and areas are possible. Irrespective of the collision angle, the graphene sheets need to overcome the dominant energy barrier resulting from the last layer of confined solvent molecules, as discussed above. Therefore, the ensemble average of all collision angles can be viewed as an effective face-to-face collision that we have considered in our analysis,

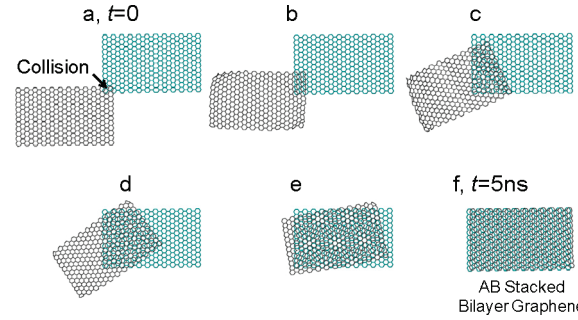

Figure 7. MD simulations of the recombination of two single-layer graphene sheets in NMP solvent. When the two sheets collide within a very small area, the very strong vdW forces between the graphene sheets induce recombination of the two sheets within 5 ns.

where the radial coordinate, r, corresponds to the intersheet separation d calculated using MD simulations. We note that the ensemble does not include events associated with perpendicular and edge-to-edge collisions, but we assume that for relatively large graphene dispersions in dilute solutions, these events are quite rare in comparison with the face-to-face collisions considered here. Consequently, the intersheet interaction potential energy, V, was further simplified as follows:[57]

$$V = \Phi A_C \quad (16)$$

where Φ is the PMF per unit area between two parallel graphene sheets obtained by least-squares fitting of eq 1 to the MD simulation results and A_C is the average collision area, which is the *only adjustable parameter* in our model. For given values of the parameter A_C and the initial concentrations of multilayer graphene sheets, N_{bi0}, the time-dependent concentrations of graphene sheets, $N_{bi}(t)$, can be obtained by simultaneously solving eqs 1, 12, 13, 15, and 16 numerically. For the limiting case where only single-layer graphene sheets are present initially (i.e., $N_{bi0} = 0$ for $i > 1$), the aggregation process modeled above is exactly analogous to a step-polymerization reaction.[58] In that case, $N_{bi}(t)$ as a function of time t can be expressed analytically as follows:[58]

$$N_{bi}(t) = N_{b10}\left(\frac{1}{1 + N_{b10}kt}\right)^2\left(\frac{N_{b10}kt}{1 + N_{b10}kt}\right)^{i-1} \quad (17)$$

When the graphene sheet possesses higher kinetic energy, it can overcome a higher energy barrier. Therefore, the average collision area, A_C, can be larger. We therefore expect A_C to depend primarily on the solution temperature. Once two graphene sheets overcome the energy barrier and collide in a small area, very strong vdW forces will drive the two sheets to recombine, thus inducing desorption of solvent molecules residing on the contact surfaces. This claim was verified by carrying out MD simulations on two single-layer graphene sheets solvated in NMP solvent with a very small initial collision area (0.27 nm^2), as shown in Figure 7. During the recombination process, the two graphene sheets always aimed to maximize their contact area and form the most thermodynamically stable AB-stacked bilayer graphene within 5 ns. Notably, for most coagulation processes taking place in dilute colloidal dispersions,

(57) Girifalco, L. A.; Hodak, M.; Lee, R. S. *Phys. Rev. B* **2000**, *62*, 13104–13110.
(58) Dotson, N. A.; Galvan, R.; Laurence, R. L.; Tirrell, M. *Polymerization Process Modeling*; Wiley-VCH: Weinheim, Germany, 1996.

the relevant time scale is associated primarily with a diffusion-controlled process rather than with a recombination (reaction)-controlled process following the "collision" between two colloids. Therefore, the actual time scale associated with the coagulation of graphene is expected to be much longer than 5 ns.

The collision area A_C can be obtained by fitting the predicted time-dependent graphene layer distribution to that measured experimentally. To illustrate this procedure, we made use of the recent work by Hernandez et al.,[15] who studied the dispersion of pristine graphene sheets in NMP solvent. For the aggregation of large graphene sheets in NMP solvent, we assumed that all of the graphene sheets had the same area, 1 μm^2, which is the average area observed by transmission electron microscopy. Therefore, the weight of single-layer graphene sheets (4.7×10^8 g/mol) could be obtained. On the basis of (i) the raw graphite concentration (0.1 mg/mL), (ii) the fraction of material remaining after centrifugation (7%), and (iii) the single-layer number fraction (27%) in pure NMP solvent at $t = 0$, all reported by Hernandez et al.,[15] the initial concentration of single-layer graphene sheets, N_{b10}, was calculated to be 1.05×10^{15} m^{-3}. In addition, by assuming a Gaussian distribution to fit the experimentally observed graphene layer distribution at $t = 0$,[24] we obtained the initial concentration of multilayer graphene sheets shown in Figure 8a. The parameter A_C was then calculated by least-squares fitting of the experimentally reported single-layer number and mass fractions of graphene sheets as a function of time and solving eqs 1, 12, 13, 15, and 16 iteratively. The nonlinear minimization algorithm for the least-squares fitting was carried out utilizing the interior-reflective Newton method subroutine[59] in the MATLAB numerical library. Figure 8b compares the fit of our kinetic aggregation model using the best-fit A_C value (0.0284 nm^2) to the experimental results of Hernandez et al.[15] With only the single fitted parameter A_C, our current model fit the experimental data nicely. This suggests that our theoretical methodology, which combines the theory of slow colloid aggregation with MD simulations, is capable of predicting the colloidal stability of graphene sheets in polar solvents. The predicted time-dependent distribution of graphene layers in NMP (Figure 8c) clearly shows that graphene sheet aggregation shifts the distribution in the direction of thicker layers as time evolves. In particular, the fraction of single-layer gaphene, which is 27% at $t = 0$, is reduced to 9% in 10 days. In addition, the initially dominant concentrations of single-layer and two-layer graphene sheets decrease significantly with time, while the overall distribution becomes flat in 1 month. For the 3 month graphene/NMP solution, the suspended graphene sheets consist of only 5% single-layer graphene sheets and over 60% thick-layer ($i \geq 5$) graphene sheets. We can therefore conclude that even for the broadly utilized, relatively efficient solvent NMP, the degradation of thin-layer graphene content with time is quite considerable. Consequently, to utilize solvents in future dispersion applications involving graphene, both storage and processing times have to be carefully controlled to obtain better yields.

By making use of the fitted parameter A_C corresponding to NMP as well as of the PMF expressions obtained using MD simulations for the four other solvents considered, our kinetic aggregation model can also predict the stability of graphene in DMF, GBL, DMSO, and water. Assuming the same initial graphene layer distribution used for NMP (Figure 8a), we carried out similar calculations for the other four solvents. Specifically, Figure 9 shows the calculated concentrations of single-layer graphene sheets for all five solvents as functions of time. If one defines the lifetime of liquid-phase graphene as the time required for the concentration of single-layer graphene sheets to be reduced by half, the lifetimes for NMP, DMSO, DMF, GBL, and water are 31.4, 30.7, 27.4, 11.3, and 4.3 h,

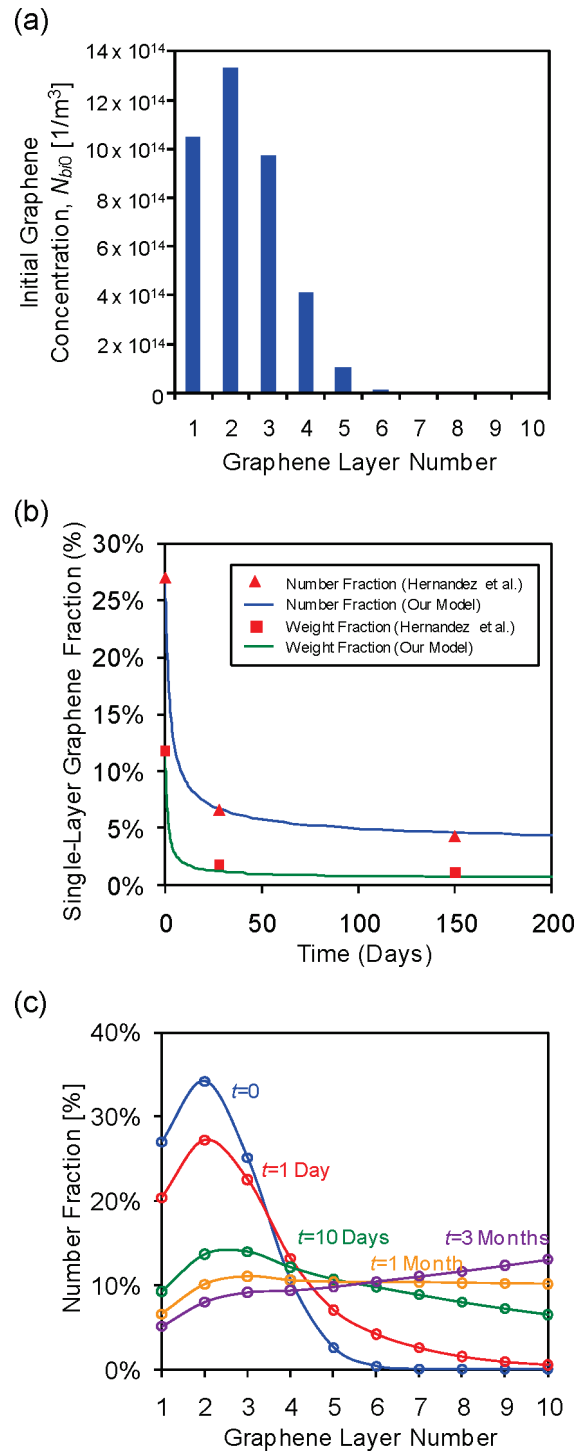

Figure 8. (a) Calculated initial layer distribution of graphene sheets in NMP solvent based on the experimental work reported by Hernandez et al.[15] (b) Experimental number fraction and weight fraction of single-layer graphene sheets (symbols) and those calculated using our current kinetic aggregation model with the best-fit parameter A_C (solid lines) as functions of time. (c) Predicted distributions of graphene layer number fraction in NMP solvent at different times.

(59) Coleman, T. F.; Li, Y. Y. *SIAM J. Optimization* **1996**, *6*, 418–445.

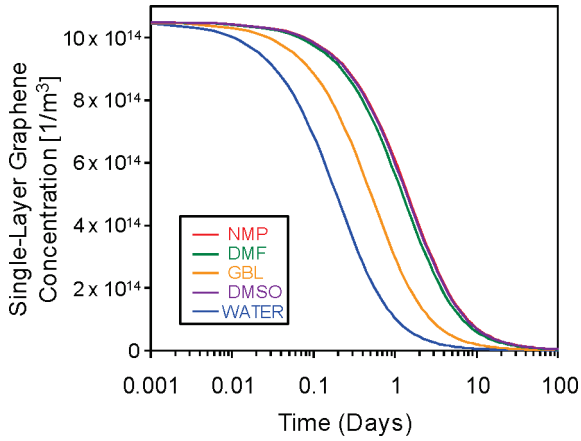

Figure 9. Numerically predicted concentrations of single-layer graphene sheets in the five solvents as functions of time.

respectively. According to the predicted lifetimes, the ranking of the five solvents in terms of their ability to efficiently disperse graphene in a stable manner is as follows: NMP ≈ DMSO > DMF > GBL > water. It is very encouraging to see that the solvents most commonly used in experiments involving the dispersion of graphene are NMP, DMSO, and DMF,[9] consistent with our predicted lifetimes. We stress that because the aggregation reaction is second-order, the lifetimes of the graphene sheets also depend on their concentrations. Therefore, the lifetimes reported here are suitable only for the specific experiments carried out by Hernandez et al.[15] Nevertheless, our predicted solvent ranking should remain valid.

4. Conclusions

The mechanism of stabilization of liquid-phase-exfoliated graphene sheets in polar solvents has been investigated using MD simulations. In addition, a kinetic theory of colloid aggregation to quantify the lifetime of suspended graphene has been proposed. For the five solvents considered (NMP, DMF, DMSO, GBL, and water), the graphene sheets are predicted to aggregate on the basis of thermodynamic arguments. Specifically, according to the simulated PMF as a function of intersheet separation, this is due to fact that the enormous vdW interactions that operate between the graphene sheets are responsible for the lowest energy minimum in the PMF. Nevertheless, because of the different affinities of each solvent for the surface of graphene, efficient solvents can enhance the stability of the graphene sheets by (i) reducing the depth of the vdW well and (ii) increasing the energy barrier. We have found that the dominant energy barrier results from the interactions of a single layer of confined solvent molecules with the two parallel graphene sheets. More specifically, prior to the desorption of the confined single layer of solvent molecules, the increase in the steric repulsions between the solvent molecules and graphene is the origin of the energy barrier responsible for repelling the graphene sheets. Therefore, when the interactions between graphene and the confined solvent molecules are stronger, the solvent molecules prefer to be confined in a narrower intersheet space, resulting in a higher energy barrier that hinders recombination of the graphene sheets. In order to stabilize confined solvent molecules to stabilize graphene, an efficient, molecular-level design of a solvent would involve tuning its chemical structure in such a way that the solvent−graphene interaction energy is much lower than the bulk solvent−solvent interaction energy.

To describe the aggregation of graphene sheets in a solvent, we have proposed a kinetic model based on the slow aggregation theory of colloids. The PMF calculated from MD simulations can be utilized as the interparticle potential energy in the kinetic model presented here. With only one adjustable parameter, the average collision area, which can be estimated from experimental data, our theory can fit the experimentally observed time-dependent fractions of single-layer graphene sheets reasonably well. By combining the kinetic aggregation model and the calculated PMF curves for the five solvents considered, we were able to calculate the lifetimes of graphene sheets and rank the five solvents in terms of their ability to stabilize graphene. Specifically, the predicted ranking is NMP ≈ DMSO > DMF > GBL > water, which is consistent with the widespread use of the first three solvents to disperse graphene.

The mechanism and theoretical methodology presented here are expected to be very useful in shedding light on the ability of polar solvents to disperse graphene as well as in allowing a quantitative estimation of the stability of liquid-phase-exfoliated graphene as reflected in the lifetimes. In addition, we hope that the molecular-level design of better solvents to disperse graphene will be facilitated by the fundamental principles and theoretical methods presented here.

Acknowledgment. C.-J.S. is grateful for partial financial support from the David H. Koch Fellowship. S.L. and D.B. are grateful for the financial support from the DuPont/MIT Alliance. M.S.S. acknowledges funding from the 2009 U.S. Office of Naval Research Multi University Research Initiative (MURI) on Graphene Advanced Terahertz Engineering (GATE) at MIT, Harvard, and Boston University. M.S.S. is also grateful for a 2008 Young Investigator Program (YIP) Award from the U.S. Office of Naval Research. We are grateful to Richa Sharma and Aravind Vijayaraghavan for helpful discussions.

Supporting Information Available: Detailed partial charge information for DMF and DMSO (Table S1), best-fit values of the parameters in eq 1 for the five solvents (Table S2), and complete ref 15. This material is available free of charge via the Internet at http://pubs.acs.org.

JA1064284